Ultrasonic Measurements of Anisotropy of Shales

Malleswar "Moe" Yenugu

School of Geology and Geophysics, University of Oklahoma, USA

Abstract

Seismic anisotropy is the variation of wave speed along different directions in a material. Preferential mineral alignment, layering, and fracturing all cause seismic anisotropy observed in many crustal rocks. Shales are the most abundant lithology in a sedimentary basin and exhibit a relatively large degree of anisotropy. Ultrasonic measurements are carried out on an outcrop of Green River shale to study its anisotropy. The elastic constants and Thomsen parameters are calculated and plotted against the effective pressure on a suite of three plugs of the Green River shale. The variation of velocities on different plugs of the same suite indicates that the Green River shale is anisotropic.

Introduction

Shales and silts are the most abundant sedimentary rocks in the earth's crust. In petroleum geology, organic shales are source rocks as well as seal rocks that trap oil and gas. In reservoir engineering, shales are flow barriers. In drilling, the bit often encounters greater shale volumes than reservoir sands. In seismic exploration, shales interfacing with other rocks often form good seismic reflectors. As a result, seismic and petrophysical properties of shales and the relationships among these properties are important for both exploration and reservoir management.

Anisotropy factors in a first order way into seismic imaging and attribute analyses. Consequences of ignoring anisotropy has lead to drilling of a good number of dry holes where anomalies are caused by shale on shale or anisotropic shale over or under sands (Margesson and Sondergeld, 1998). The magnitude of anisotropy in shales varies considerably and has been measured to be as much as 42% in shear velocity (Sondergeld and Rai, 1992) and 38% in P-wave (Hornby et al., 1999).

What is Anisotropy?

A material is anisotropic if the value of a vector measurement of a rock property varies with direction. Anisotropy is widely occurring phenomenon cutting across diverse disciplines of Petroleum industry. Where anisotropy arises, many convenient assumptions fail. Seismic reflectors appear at wrong depths. Seismic lines donot tie. Waterflood programs fail. Induction logs are misinterpreted and water sands are mistaken for pay. Different disciplines of oil industry treat anisotropy in different ways. Geophysicists generally focus on variation of seismic wavefront velocity or on the polarization of shear waves. Petrophysicists may measure resistivity anisotropy. Drillers and geologists may think first of anisotropy in rock strength or stiffness produced by earth stresses. Stratigraphers may concentrate on anisotropy of magnetic properties and reservoir engineers need go to great lengths to characterize permeability anisotropy to plan an optimal production strategy.

Causes of Anisotropy

Anisotropy in sediments may develop during deposition or post deposition. In clastic sediments, anisotropy can arise both during and after deposition. In carbonates, anisotropy is controlled mostly by fractures and diagenetic processes, and so tends to arise after deposition. For anisotropy to develop during deposition of clastics, there needs to be an ordering of sediments-in essence, some degree of homogeneity, or uniformity from point to point. If a rock were heterogeneous in the five fundamental properties of its grains- composition, size, shape, orientation and packing- anisotropy cannot develop because there would be no directionality intrinsic to the material. Anisotropy at the bedding scale that arises during deposition therefore may have two causes. One is a periodic layering, usually attributed to changes in sediment type, typically producing beds of varying material or grain size. Another results from the ordering of grains induced by the directionality of the transporting medium. Anisotropy is therefore governed not only by variation in the type of material but also by variation in its arrangement and grain size.

The main cause of elastic anisotropy in shales appears to be layering of clay platelets (Figure 1) on the micron scale due to geotropism -turning in the earth's gravity field – and compaction enhances the effect.

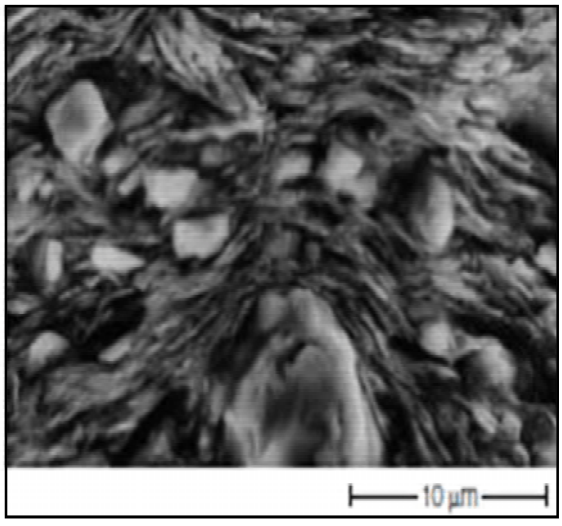

Fig.1 Photomicrograph of shale showing clay platelets distributed

Types of Anisotropy

There are two styles of alignment in earth materials – horizontal and vertical and they give rise to two types of anisotropy. In the simplest horizontal, or layered case, elastic properties may vary vertically, such as from layer to layer, but not horizontally (Figure 2). Such a material is called transversely isotropic with a vertical axis of symmetry (TIV) (Figure 2). Waves generally travel faster horizontally, along layers, than vertically. Detecting and quantifying this type of anisotropy are important for correlation purposes, such as comparing sonic logs in vertical and deviated wells, and for borehole and surface seismic imaging and studies of amplitude variation with offset (AVO).

The simplest case of the second type of anisotropy corresponds to a material with aligned vertical weaknesses such as cracks or fractures, or with unequal horizontal stresses. Elastic properties vary in the direction crossing the fractures, but not along the plane of the fracture. Such a material is called transversely isotropic with a horizontal axis of symmetry (TIH) (Figure 2). Waves traveling along the fracture direction generally travel faster than waves crossing the fractures. Identifying and measuring this type of anisotropy yield information about rock stress, fracture density and fracture orientation. These parameters are important for designing hydraulic fracture jobs and for understanding horizontal and vertical permeability anisotropy.

Acoustic Anisotropy - Shear wave splitting

Laboratory measurements of ultrasonic velocities have confirmed that compressional waves travel faster in the direction of applied stress. The reason may be that all rocks contain some distribution of microcracks. As stress is applied, cracks oriented normal to the direction of greatest stress will close, while cracks aligned with the stress direction will open (Figure 3). In most cases, waves travel fastest when their particle motion is aligned in the direction of the opening cracks.

A noticeable feature of acoustic anisotropy is shear wave splitting, or polarization, typically caused by fractures. If polarization of a shear wave is not parallel to the strike of a fracture set, the wave will be split into two components as it passes through the fractures (Figure 4). The first, faster component will have particle motion aligned parallel to the fracture strike. A second, slower component will have particle motion aligned perpendicular to the fracture strike (Figure 4).

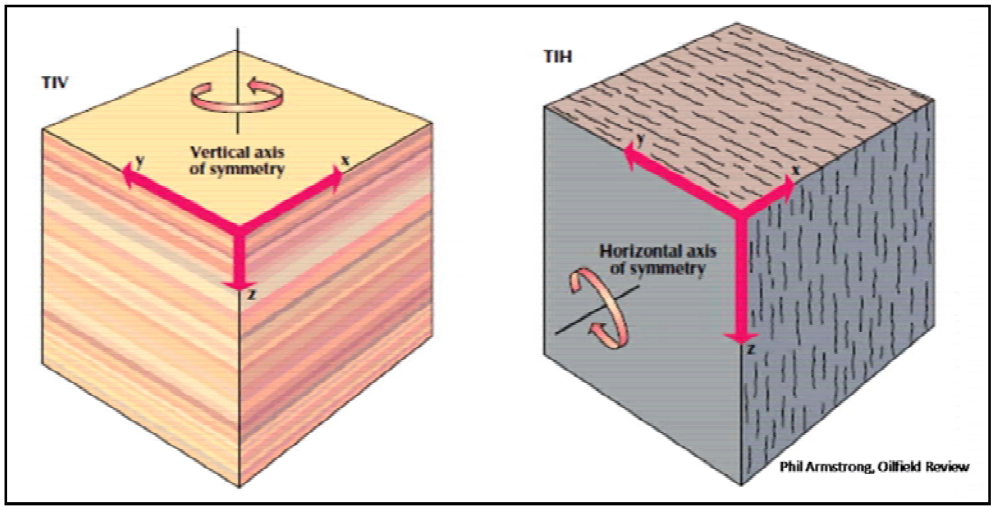

Fig.2 Two types of anisotropy (TIV and TIH)

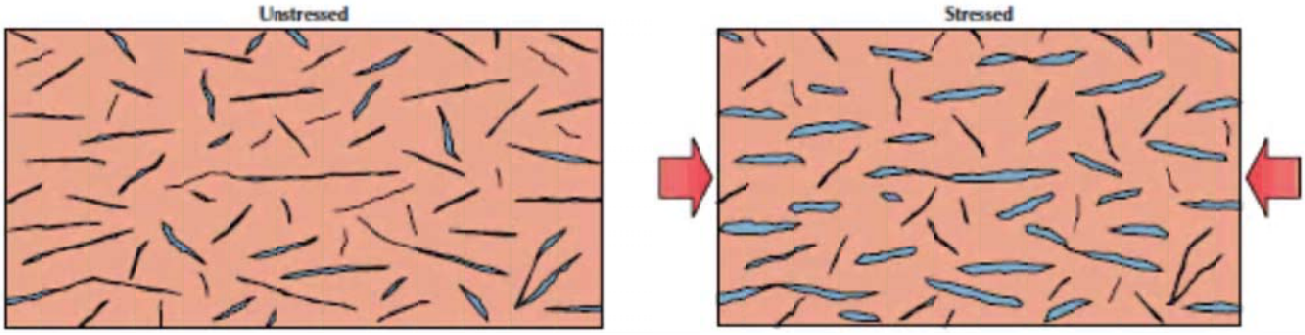

Fig. 3 Effect of non-uniform compressive stress on microcracks (Armstrong, 1994)

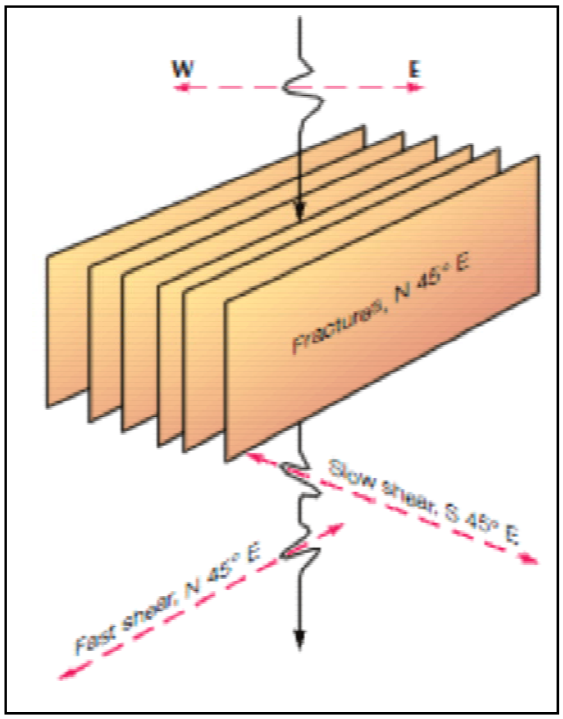

Fig. 4 Figure showing how fractures split shear waves – shear wave splitting. (Anderson et al, 1994)

Laboratory Measurements of Seismic Anisotropy

The data on elastic properties of shales are scarce which is primarily for two reasons: obtaining and preserving shale samples is difficult, and taking measurements is time consuming. To obtain elastic constants, velocities and anisotropies in shales are traditionally measured on multiple adjacent core plugs with different orientations. For example, for a transversely isotropic (TI) rock, three plugs must be measured separately, one parallel, one perpendicular, and one at 45 degree to the symmetry axis in order to derive the five independent elastic constants (Vernik et al., 1994).

Figure 5 shows the three-plug method of TI measurements in the laboratory. Three plugs are drilled adjacently from a full-diameter core: one at 0 degree (vertical plug), second at 90 degree (horizontal plug), and third at 45 degree to the symmetry axis. The velocities and densities measured on these core plugs yield the elastic constants C33 and C44, C11 and C66, and C13 respectively. The advantage of this three-plug method is redundancy for calculations of the five independent elastic constants since each core plug measurement yields three velocities (one P and two S).

Ultrasonic velocity measurements are carried out on an outcrop of the Green shale. I cut three plugs in the laboratory as shown in the Figure 5 and measured their densities and porosities which are shown in the Table 1.

Table 1: Densities and porosities of the three plugs

Orientation	Dry Density (gr/cc)	Grain Density (gr/cc)	Saturated Density (gr/cc)	Porosity %
V	0.935	1.87	1.435	0.50
H	1.358	1.94	1.658	0.30
45^0	1.309	1.87	1.609	0.30

I measured the dry and wet velocities using the pulse transmission method. Figure 6 shows apparatus set up used to measure the velocities on the samples. However, before measurements could be done, there were a few procedures to be followed:

(a) Need to enter all information about the samples, including assigning a unique ID for each sample, with the corresponding sample name and depth.

(b) After all the necessary information is entered in the computer, the samples are then placed in the transducer assembly at appropriate positions.

(c) The transducer assembly with the samples is loaded into one of the positions of the two cells of the velocity station.

(d) The cell system is properly closed. The experiment is started by filling the cells with mineral oil removing any air present. Then the system is closed and confining pressure increases as oil is pumped into the vessel.

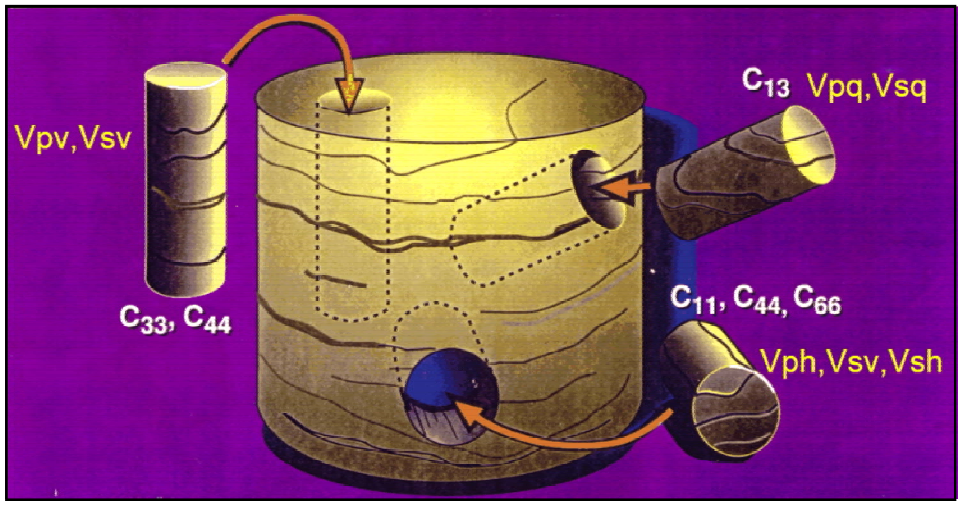

Fig. 5 Schematic showing the three-plug method for anisotropic measurements

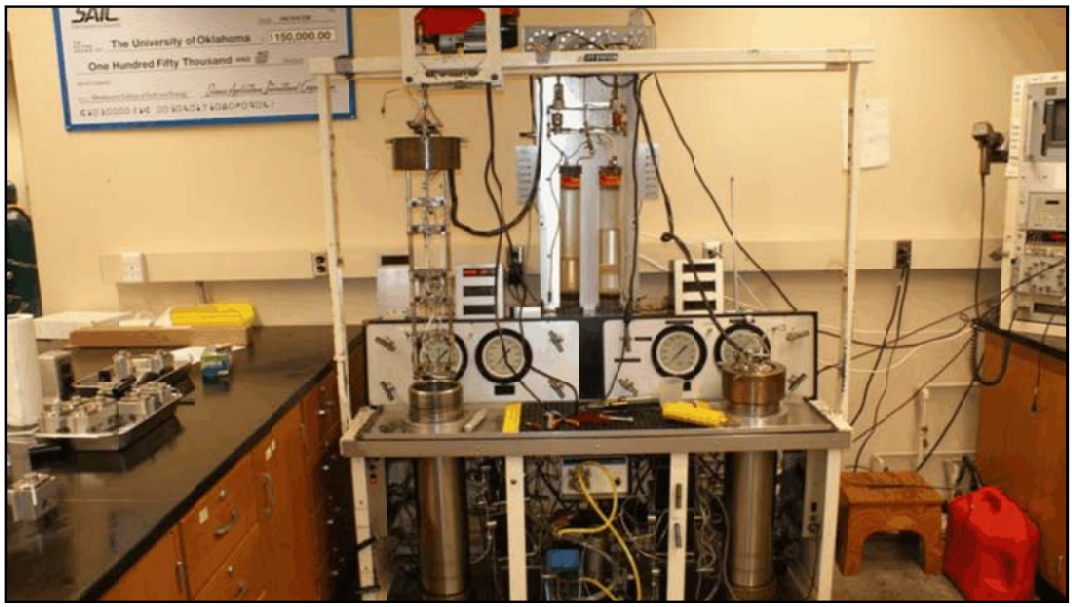

Fig. 6 Picture showing the apparatus used for Pulse-Transmission method (OU-IC^3 lab).

(e) Pore pressure is kept at atmospheric condition for all measurements so the confining pressure corresponds to effective pressure as the nine (effective) pressures 250, 500, 750, 1000, 1500, 2000, 3000, 4000, and 5000 psi.

(f) For data analysis, recorded data are transferred to a computer workstation and first arrivals are picked from the following transmitter-receiver pairs: P-P, S1-S1, and S2-S2.

Results

Initially the ultrasonic measurements are carried out on dry plugs following the above procedure. The results are shown in the Table 2.

S wave splits into two different S waves, namely Sv and Sh. We can only measure Sv for vertical plug (here assigned as Vsv1) and can measure both Sv and Sh for

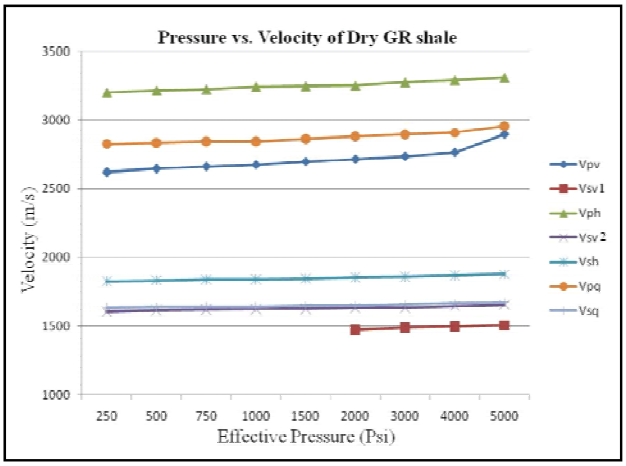

Fig. 7 Plot showing increase in velocities with increasing effective pressure.

Table 2: Results of ultrasonic measurements of velocities on the three plugs (dry) for increasing pressure. The first subscript 'p' stands for pressure wave and 's' for shear wave; the second subscript 'v' stands for vertical plug (v1 for vertical and v2 for horizontal), 'h' for horizontal plug and 'q' for the plug at 45 degrees.

Effective Pressure (psi)	For vertical plug		For horizontal plug			For 45 degree plug	
	Vpv (m/s)	Vsv1 (m/s)	Vph (m/s)	Vsv2 (m/s)	Vsh (m/s)	Vpq (m/s)	Vsq (m/s)
250	2622	0	3203	1607	1827	2827	1635
500	2648	0	3217	1616	1834	2834	1637
750	2662	0	3225	1619	1839	2845	1639
1000	2675	0	3244	1623	1842	2845	1640
1500	2699	0	3248	1625	1845	2863	1646
2000	2716	1475	3253	1632	1854	2882	1649
3000	2737	1487	3277	1635	1860	2897	1656
4000	2766	1498	3291	1645	1869	2908	1665
5000	2896	1505	3310	1655	1877	2957	1674

Table 3: Variation in five elastic constants for dry samples derived from velocities and densities for increasing pressure.

Pressure (psi)	$C_{33}=\rho V_{pv}^2 \times 10^6$ Pa	$C_{44}=\rho V_{sv}^2 \times 10^6$ Pa	$C_{11}=\rho Vph^2 \times 10^6$ Pa	$C_{66}=\rho Vsh^2 \times 10^6$ Pa	$C_{13} \times 10^6$ Pa
250	6.42	3.50	13.93	4.53	2.68
500	6.55	3.54	14.05	4.56	2.57
750	6.62	3.55	14.12	4.59	2.65
1000	6.69	3.57	14.29	4.60	2.44
1500	6.81	3.58	14.32	4.62	2.67
2000	6.89	3.61	14.37	4.66	2.87
3000	7.01	3.63	14.58	4.69	2.89
4000	7.15	3.67	14.70	4.74	2.84
5000	7.84	3.71	14.87	4.78	3.25

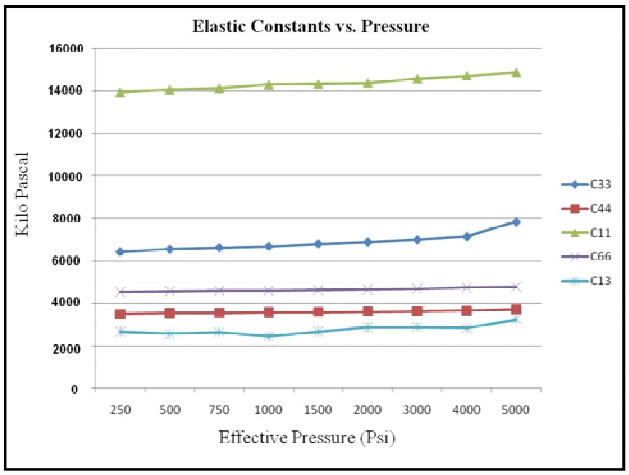

Fig.8 Five independent elastic constants plotted against effective pressure for dry samples.

Anisotropic Constants :

$$\alpha = \sqrt{\frac{C_{33}}{\rho}} \quad \text{..... (6)}$$

$$\beta = \sqrt{\frac{C_{44}}{\rho}} \quad \text{..... (7)}$$

$$\varepsilon = \frac{C_{11}-C_{33}}{2C_{33}} \quad \text{..... (8)}$$

$$\gamma = \frac{C_{66}-C_{44}}{2C_{44}} \quad \text{..... (9)}$$

$$\delta = \frac{(C_{13}+C_{44})^2-(C_{33}-C_{44})^2}{2C_{33}(C_{33}-C_{44}} \quad \text{..... (10)}$$

horizontal plug (assigned as Vsv2 and Vsh). Velocity changes with increasing pressure on the samples. Velocities are plotted against increasing pressure in Figure 7.

All the five independent elastic constants are computed from velocities and bulk density of the samples. The elastic constants are

$$\rho V^2_{pv} = C_{33} \quad \text{..... (1)}$$

$$\rho V^2_{sv} = C_{44} \quad \text{..... (2)}$$

$$\rho V^2_{ph} = C_{11} \quad \text{..... (3)}$$

$$\rho V^2_{sh} = C_{66} \quad \text{..... (4)}$$

$$4\rho V^2_{ph} = C_{11} + C_{33} + 2C_{44} + [(C_{11} - C_{33})2 + (C_{13} + C_{44})^2]^{1/2} \quad \text{..... (5)}$$

.....

$C_{33} > C_{44}$

$C_{11} > C_{33}$

The values of five elastic constants for increasing effective pressure computed from the velocities and densities using the above Equations 1 – 5, are shown in Table 3 and plotted in Figure 8.

I computed the standard five Thomsen anisotropic parameters using the above five elastic constants and the Equations 6 - 10 shown below. The results are shown in Table 4 and plotted against pressure in Figure 9.

Table 4: Five Thomsen anisotropic parameters derived from the five elastic constants

Pressure (psi)	α (m/s)	β (m/s)	ε	γ	δ
250	2622	1936.69	0.58	0.15	0.79
500	2648	1947.54	0.57	0.14	0.72
750	2662	1951.15	0.57	0.15	0.72
1000	2675	1955.97	0.57	0.14	0.64
1500	2699	1958.38	0.55	0.14	0.66
2000	2716	1966.82	0.54	0.15	0.69
3000	2737	1970.43	0.54	0.15	0.66
4000	2766	1982.49	0.53	0.15	0.61
5000	2896	1994.54	0.45	0.14	0.49

The dry samples are pressurized upto 2000 psi with brine and kept for two days. The same procedure of Pulse-Transmission method is followed to measure the ultrasonic velocities, elastic constants and the anisotropic parameters. The results are shown in Tables (5, 6 and 7) and also plotted in Figures 10, 11 and12.

Table 5: Results of ultrasonic measurements of velocities on the three plugs (brine saturated) for increasing pressure. The first subscript 'p' stands for pressure wave and 's' for shear wave; the second subscript 'v' stands for vertical plug (v1 for vertical and v2 for horizontal), 'h' for horizontal plug and 'q' for the plug at 45 degrees.

Effective Pressure (psi)	For vertical plug		For horizontal plug			For 45 degree plug	
	Vpv (m/s)	Vsv1 (m/s)	Vph (m/s)	Vsv2 (m/s)	Vsh (m/s)	Vpq (m/s)	Vsq (m/s)
250	2597		3185		1771	2766	
500	2665		3207	1571	1781	2814	1643
750	2682	1260	3207	1583	1789	2839	1644
1000	2689	1284	3221	1588	1801	2842	1650
1500	2702	1293	3230	1597	1820	2849	1653
2000	2730	1303	3244	1605	1829	2868	1662
3000	2762	1316	3287	1620	1839	2893	1666
4000	2784	1327	3296	1633	1847	2912	1676
5000	2810	1335	3326	1683	1853	2939	1681

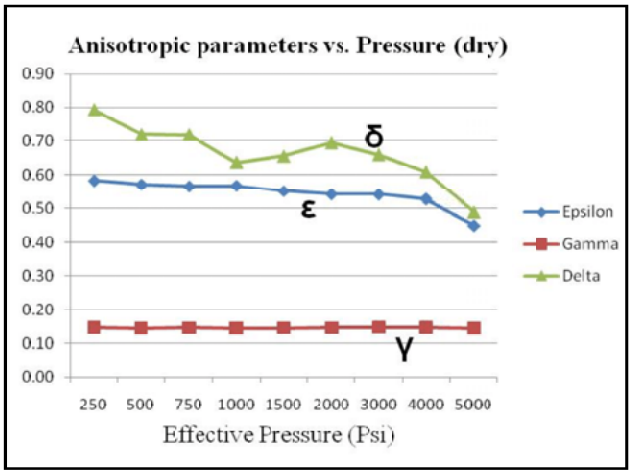

Fig.9 Thomsen anisotropic parameters vs. effective pressure (dry samples).

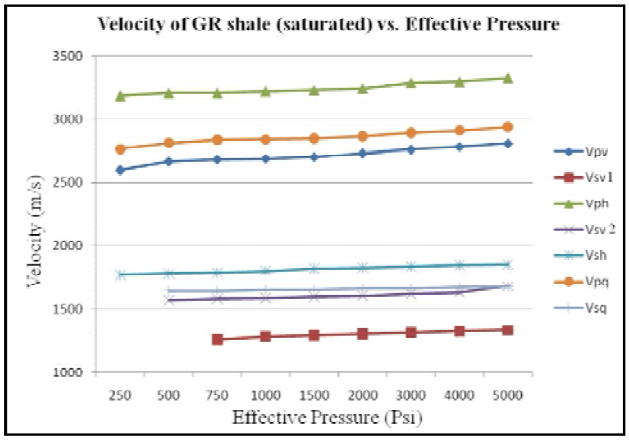

Fig. 10 Velocities plotted against increasing effective pressure. The first subscript 'p' stands for pressure wave and 's' for shear wave; the second subscript 'v' stands for vertical plug, 'h' for horizontal plug and 'q' for the plug at 45 degrees.

Table 6: Five elastic constants for brine saturated samples.

Pressure (psi)	$C_{33}=\rho V_{pv}^2 \times 10^6$ Pa	$C_{44}=\rho V_{sv}^2 \times 10^6$ Pa	$C_{11}=\rho Vph^2 \times 10^6$ Pa	$C_{66}=\rho Vsh^2 \times 10^6$ Pa	$C_{13} \times 10^6$ Pa
250	9.67	4.28	16.81	5.20	1.84
500	10.19	4.32	17.05	5.25	2.37
750	10.32	4.34	17.05	5.30	2.80
1000	10.37	4.36	17.20	5.37	2.68
1500	10.47	4.37	17.29	5.49	2.69
2000	10.69	4.41	17.44	5.54	2.81
3000	10.94	4.43	17.91	5.60	2.84
4000	11.12	4.48	18.01	5.65	2.99
5000	11.33	4.54	18.34	5.69	3.11

Table 7: Showing the calculated anisotropic parameters (saturated).

Pressure (psi)	α (m/s)	β (m/s)	ε	γ	δ
250	2597	1727.36	0.37	0.11	0.08
500	2665	1737.03	0.34	0.11	0.09
750	2682	1740.26	0.33	0.11	0.13
1000	2689	1744.56	0.33	0.12	0.11
1500	2702	1746.71	0.33	0.13	0.10
2000	2730	1754.23	0.32	0.13	0.10
3000	2762	1757.45	0.32	0.13	0.07
4000	2784	1768.20	0.31	0.13	0.08
5000	2810	1778.95	0.31	0.13	0.08

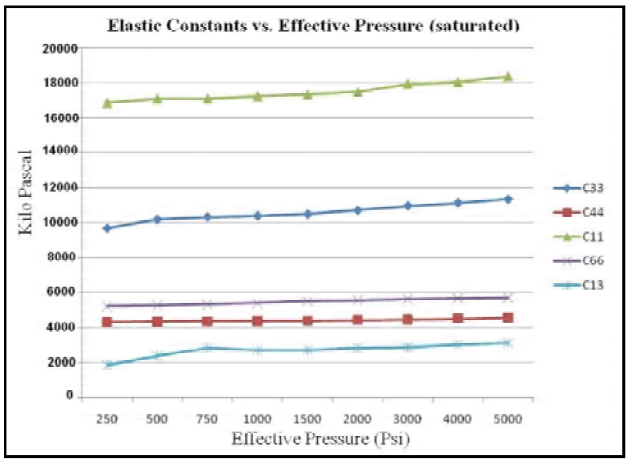

Fig. 11 Five independent elastic constants plotted against effective pressure for brine saturated samples. Compare with the results for the dry samples shown in Figure 8.

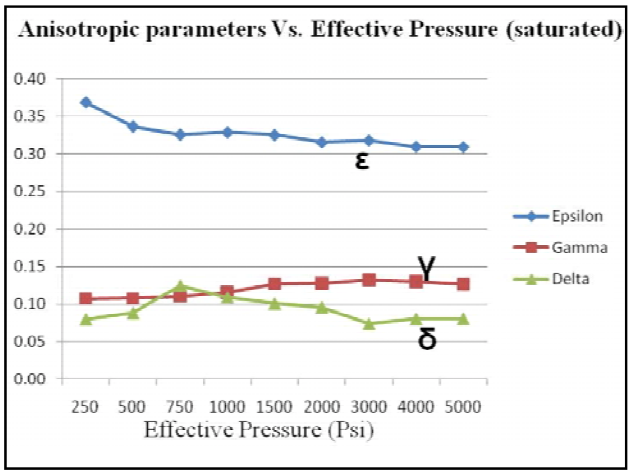

Fig. 12 Thomsen anisotropic parameters vs. effective pressure (brine saturated samples). Compare with the results for dry samples shown in Figure 9.

The variation of measured velocities with angles (0, 45 and 90 degrees) has been plotted at 3000 psi in Figure 13. These plots give an idea of how velocities vary with respect to the change in angle of sample cutting from the suite.

Interpretation

Not much difference of ultrasonic velocities is observed between dry and brine saturated Green River shale samples. However considerable change in velocity is observed on the three plugs taken from the same suite which indicates the anisotropy of seismic velocities in the Green River shales. The plots between the velocities and effective

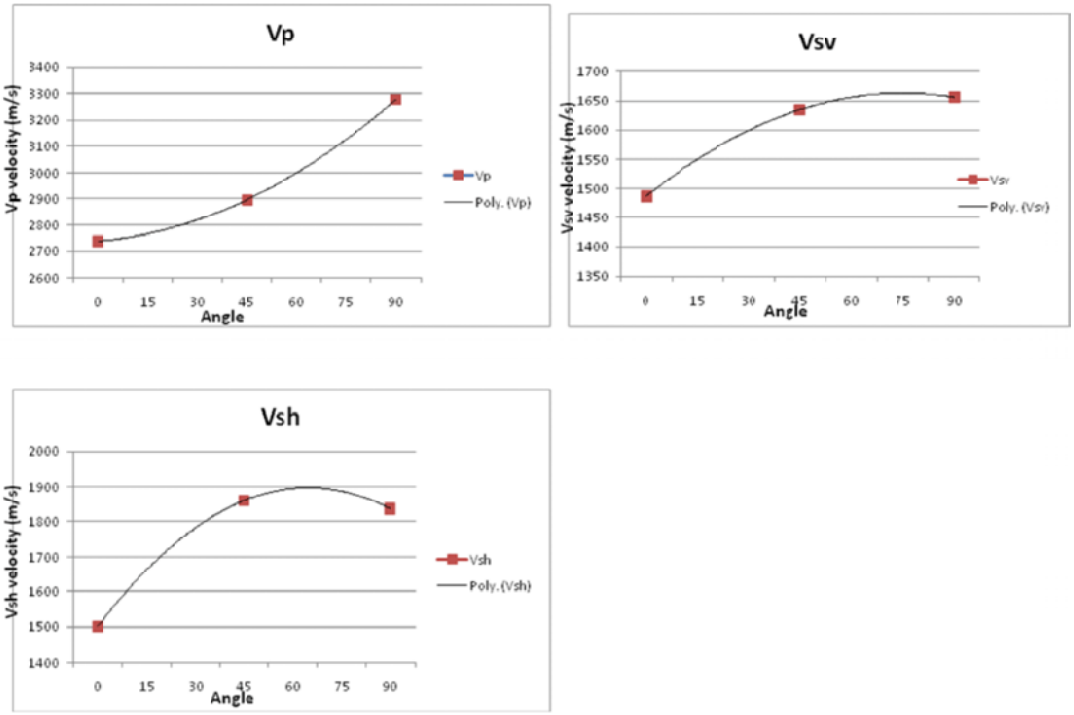

Fig. 13 Plots showing the variation of velocities with the change of angle of cutting the core plugs from the sample.

pressure clearly indicate that the shale is exhibiting anisotropy. The P and S (Sv and Sh) wave velocities are different in all the three directions of the same formation. This anisotropy may be due to grain alignment, micro-cracks etc. The magnitude of anisotropy of velocities is observed around 20-25% for P-wave velocity and 8-14% for S-wave velocities. It is observed that the P-wave anisotropy decreases with increasing pressure – both for the dry and the saturated samples. However, S-wave anisotropy remains nearly unaffected by increasing pressure for dry rock but increases for the saturated rock sample (Figures 9 and 12).

It is also observed that the velocities are continuously increasing from the pressure around 2000 psi. This may be due to the closure of the micro cracks of the sample plugs with the increase of the effective pressure. The five independent elastic constants that are measured also show trend similar to that of P and S velocities. This is not surprising since the elastic constants are derived from the velocities and densities.

The variation of velocities with the change in angle of cutting of samples is also observed by plotting the measured velocities on the three core plugs at 3000 psi (Figure 13). Vp is increasing with the increase in angle, Vsv is increasing with angle upto 75 degrees, then starts to decrease with the increase in angle. Vsh is also increasing upto 65 degrees then decreasing with the increase in angle. This variation of velocities with the increase in angles clearly shows that the Green River is elastically anisotropic.

Conclusions

Ultrasonic measurements of P & S wave velocities carried out on a suite of three plugs at different orientations from an outcrop of Green River shale has brought out the anisotropic nature of these shales. P-wave anisotropy decreases with increasing pressure-both for the dry and the saturated samples. However, S-wave anisotropy remains nearly unaffected by increasing pressure for dry rock, but increases for the saturated rock sample.

Acknowledgements

The author thanks Dr. C H Mehta for making valuable comments/suggestions to bring this manuscript into a better shape.

References

Barbara Anderson, et al, 1994, Oilfield Anisotropy: Its Origins and Electrical Characteristics: Oilfield Review, p 48-56.

Boris Gurevich, et al, 2007, Fluid substitution, dispersion, and attenuation in fractured and porous reservoirs–insights from new rock physics models: The Leading Edge, p 1162-1168.

Carl H Sondergeld, et al., 1999, Ultrasonic measurements of anisotropy on the Kimmeridge shale: SEG Expanded abstracts.

Colin M Sayers, 1999, Stress-dependent seismic anisotropy of shales: Geophysics, Vol.64, No.1, p 93-98.

Darrel Hemsing and Douglas R Schmitt, 2006, Laboratory Determination of Elastic Anisotropy in Shales from Alberta: SEG Expanded abstracts, p 229-233.

David Gray, 2005, Seismic anisotropy in coal beds: SEG Expanded abstracts, p 142-146

David Gray, 2007, Observations of Seismic Anisotropy in Prestack Seismic Data: SEG Expanded abstracts, p 119-123.

Futoshi Tsuneyama and Gary Mavko, 2005, Velocity anisotropy estimation for brine-saturated sandstone and shale: The Leading Edge, p 882-888.

Gerardo Franco and Thomas L Davis, 2007, Seismic anisotropy of tight-gas sandstones, Rulison Field, Piceance Basin, Colorado: SEG Expanded abstracts, p 1461-1465.

Ivar Brevik, et al, 2007, Documentation and quantification of velocity anisotropy in shales using wireline log measurements: The Leading Edge, p 445-451.

Jose Agnelo Soares and Margareth da Silva Brasil Guimaraes, 2003, Using Thomsen's Model to Analyze Composition and Internal Structure of Shales: AAPG International Conference, Barcelona.

Leon Thomsen, 2001, Seismic Anisotropy: Geophysics, Vol.66, No.1, p 40-41.

Manika Prasad, et al, 2009, Rock physics of the unconventional: The Leading Edge, p 34-38.

Michael Schoenberg and Colin M Sayers, 1995, Seismic anisotropy of fractured rock: Geophysics, Vol.60, No.1, p 204-211.

Michael Worthington, 2007, The compliance of macrofractures: The Leading Edge, p 1118-1122.

Phil Armstrong, et al, 1994, The Promise of Elastic Anisotropy: Oilfield Review, p 36-47.

Said Amiri Besheli, et al., 2005, The effect of seismic anisotropy on reservoir characterization: SEG Expanded abstracts, p 150-154.

Yongyi Li, 2004, Anisotropic Parameter Prediction in Clastic Rocks: CSEG National Convention, p 1-5.

Yongyi Li, 2005, Seismic Anisotropy in Overburden: CSEG National Convention, p 15-16.